ISSN 1674-1056
http://cpb.iphy.ac.cn
http://iopscience.iop.org/cpb
中国物理 B
Chinese Physics
中国物理
Chinese Physics B

Design of multi-band metasurface antenna array with low RCS performance

Si-Ming Wang(王思铭), Jun Gao(高军), Xiang-Yu Cao(曹祥玉), Yue-Jun Zheng(郑月军), Tong Li(李桐), Jun-Xiang Lan(兰俊祥), Liao-Ri Ji-Di(吉地辽日)

Citation: Chin. Phys. B . 2018, 27(10): 104102. **doi:** 10.1088/1674-1056/27/10/104102

Journal homepage: http://cpb.iphy.ac.cn; http://iopscience.iop.org/cpb

What follows is a list of articles you may be interested in

Ultra-compact graphene plasmonic filter integrated in a waveguide

Baoxin Liao(廖宝鑫), Xiangdong Guo(郭相东), Hai Hu(胡海), Ning Liu(刘宁), Ke Chen(陈科), Xiaoxia Yang(杨晓霞), Qing Dai(戴庆)

Chin. Phys. B . 2018, 27(9): 094101. **doi:** 10.1088/1674-1056/27/9/094101

Ultra-thin circularly polarized lens antenna based on single-layered transparent metasurface

Kaiyue Liu(刘凯越), Guangming Wang(王光明), Tong Cai(蔡通), Wenlong Guo(郭文龙), Yaqiang Zhuang(庄亚强), Gang Liu(刘刚)

Chin. Phys. B . 2018, 27(8): 084101. **doi:** 10.1088/1674-1056/27/8/084101

Reliable approach for bistatic scattering of three-dimensional targets from underlying rough surface based on parabolic equation

Dong-Min Zhang(张东民), Cheng Liao(廖成), Liang Zhou(周亮), Xiao-Chuan Deng(邓小川), Ju Feng(冯菊)

Chin. Phys. B . 2018, 27(7): 074102. **doi:** 10.1088/1674-1056/27/7/074102

Confinement of Bloch surface waves in a graphene-based one-dimensional photonic crystal and sensing applications

Xiu-Juan Zou(邹秀娟), Gai-Ge Zheng(郑改革), Yun-Yun Chen(陈云云)

Chin. Phys. B . 2018, 27(5): 054102. **doi:** 10.1088/1674-1056/27/5/054102

Dual-band left-handed metamaterials fabricated by using tree-shaped fractal

Xu He-Xiu, Wang Guang-Ming, Wang Jia-Fu, Yang Zi-Mu

Chin. Phys. B . 2012, 21(12): 124101. **doi:** 10.1088/1674-1056/21/12/124101

Design of multi-band metasurface antenna array with low RCS performance*

Si-Ming Wang(王思铭)†, Jun Gao(高军), Xiang-Yu Cao(曹祥玉)‡, Yue-Jun Zheng(郑月军), Tong Li(李桐), Jun-Xiang Lan(兰俊祥), and Liao-Ri Ji-Di(吉地辽日)

Information and Navigation College of Air Force Engineering University, Xi'an 710077, *China*

(Received 25 May 2018; revised manuscript received 12 June 2018; published online 27 September 2018)

In this paper, a multi-band metasurface (MS) antenna array with low radar cross section (RCS) performance is proposed and measured. Firstly, a 4×4 antenna array is composed of four 2×2 Jerusalem cross structure antenna arrays working at different frequency bands, which is aimed at enhancing the bandwidth effectively. Then, each antenna can be seen as a unit of MS in spite of adding the feeding structure. Based on phase cancellation principle, the MS is arranged into a chessboard configuration in order to realize wideband RCS reduction. Thus, excellent radiation and scattering characteristics are obtained simultaneously. Simulated and measured results indicate that this work provides a novel method to achieve bandwidth expansion as well as wideband RCS reduction of the antenna array.

Keywords: multi-band, metasurface (MS) antenna array, radar cross section (RCS) reduction, radiation

PACS: 41.20.Jb, 73.20.Mf **DOI:** 10.1088/1674-1056/27/10/104102

1. Introduction

Metasurface antenna, a new form of the combination of metamaterials and radiator, has experienced an unparalleled development in recent years. Because of its distinct advantages, such as low-profile, light weight and feasibility to realize the control of some exotic electromagnetic properties, plenty of excellent researches have been conducted.[1–4]

Nowadays, the application of metasurface (MS) has developed to a certain extent. Various MSs have been proposed, such as artificial magnetic conductor (AMC),[5,6] frequency selective surface (FSS),[7] polarization conversion metasurface (PCM),[8] etc, providing multiple potential for enhancing the radiation and reflection suppression performance. Among them, the AMC was employed as the magnetic ground plane to realize the bandwidth expansion and gain improvement of the patch antenna.[9] In Ref. [10], the concept of 'coding metamaterial' to manipulate electromagnetic waves and realize different functionalities was first put forward. By coding MS on the antenna array, the reflection was diffused in more directions to realize both monostatic and bistatic radar cross section (RCS) reduction.[11] Besides the scattering performance, in Refs. [12] and [13], the gain enhancement has also been achieved by employing a Fabry–Perot cavity, which was comprised of the PCM and the perfect electric conductor (PEC) ground. Meanwhile, chessboard PCM was printed on the up side of substrate in order to reduce RCS in band and out of band. In the researches mentioned above, the antennas and the MS were designed separately. Thus, the advantage of the MS, which has a planar structure so it is convenient to integrate with antenna to retain their inherent properties, has not been reflected sufficiently. In Ref. [14], a 2×2 MS-based circularly polarized high gain patch antenna array was proposed. In spite of its integration design, the two-layer structure increased the difficulty in being fabricated, and the scattering performance has not been mentioned. In Ref. [15] put forward was a multifunctional artificial electromagnetic surface (AEMS) in which the radiation and scattering properties both are taken into consideration. However, only two antennas working at different frequency bands were utilized, thus its working frequency band was restricted.

Inspired by the researches mentioned above, a novel design of multi-band MS antenna array with low RCS performance is proposed in this work. The 4×4 antenna array, composed of four 2×2 Jerusalem cross structure antenna arrays working at different frequency bands, is aimed at obtaining multi-band radiation characteristics. Then, based on phase cancellation principle, the MS is arranged into a chessboard configuration to achieve RCS reduction. Meanwhile the inherent essence of MS elements is retained well by adding the feeding structure. Thus, the design of multi-band MS antenna array with low RCS performance comes into reality.

The rest of this paper is organized as follows. In Section 2, the design of MS unit cell is proposed, and its radiation and scattering performance are verified. The multi-band and wideband RCS reduction properties of MS antenna array are introduced in Section 3. The experimental results and their comparison with the simulation results are described in Section 4. Finally, some conclusions are drawn from the present

*Project supported by the National Natural Science Foundation of China (Grant Nos. 61471389, 61701523, and 61671464).

†Corresponding author. E-mail: 15686018665@163.com

‡Corresponding author. E-mail: xiangyucaokdy@163.com

© 2018 Chinese Physical Society and IOP Publishing Ltd

study in Section 5.

2. Design and analysis of MS antenna unit

In this work, we choose Jerusalem cross structure as the basic unit cell to constitute the MS antenna array for its wide in-phase reflection band and facility for fabrication. As figure 1 shows, the Jerusalem cross structure is patched on a metal-backed substrate with thickness $h = 3$ mm, dielectric constant $\varepsilon = 2.65$, and loss tangent $\tan\delta = 0.001$. The side length L_p of the unit is 20 mm. Then, as a source antenna, each MS antenna unit is fed directly with 50-Ω SMA coaxial feed probe piercing through the PEC ground and substrate. The four different Jerusalem cross units are denoted as M1, M2, M3, and M4 for distinction when they are seen as MS units, while as A1, A2, A3 and A4 when they are seen as antenna units. For M1(A1), the designed parameters are as follows: $a_1 = 11$ mm, $b_1 = 6.8$ mm, $c_1 = 7.5$ mm, $d_1 = 2.1$ mm and $f_{x_1} = 2.8$ mm. The MS unit cells are simulated in Ansys HFSS by using periodic boundary condition and floquet port excitation to obtain their reflection properties. In addition, full-wave numerical analysis is also conducted when studying the radiation performance of MS antenna units under radiation boundary condition and lumped port excitation.

According to previous experience, changing parameter value of an MS unit can lead to different reflection characteristics. However, in this work, the MS unit is also seen as a radiator with energy emitting. So when analyzing the MS antenna with adding a feeding structure, it is necessary to investigate the influence of the feeding position on the scattering performance. Because the four MS antenna units have similar geometric patterns, only the simulated results of M1 are given. As shown in Fig. 2(a), when f_{x_1} is no more than 3.5 mm, the relative reflection phases have little difference. But feeding position has an obvious effect on reflection phase when f_{x_1} is greater than 3.5 mm under x polarization. In Fig. 2(b), the low reflection magnitudes indicate the evident wave absorbed by the 50-Ω impedance matching, which conduces to the achieving of good scattering performance. Because the antenna is fed at the place on the x axis, it is obvious that the patch is shorted at the feed point for y polarization. Thus for y-polarized incidence, feeding position has little influence on both reflection phase and magnitude as depicted in Figs. 2(c) and 2(d). What is more, the reflection magnitude is above 0.98 so the total reflection property is revealed under y polarization.

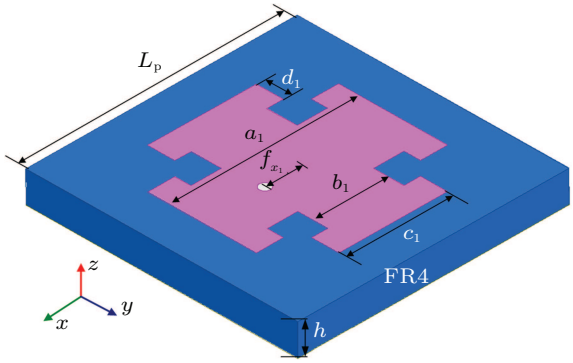


Fig. 1. (color online) Geometry of MS antenna unit M1(A1).

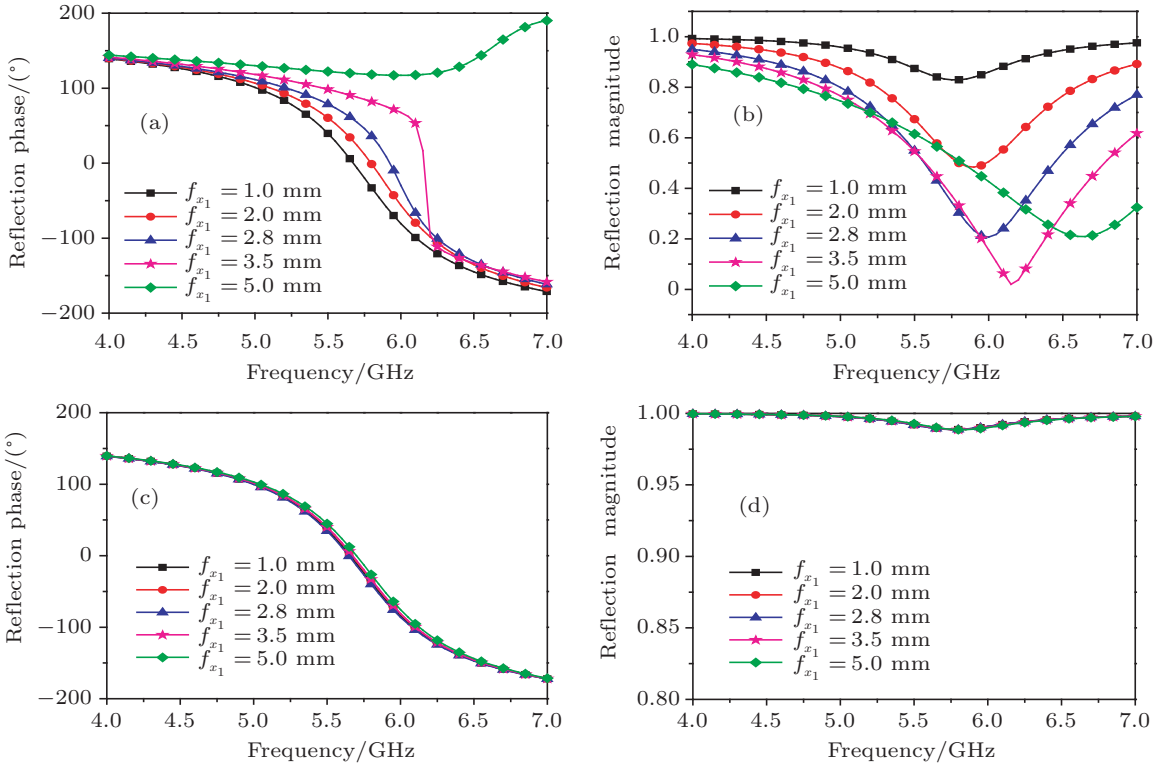


Fig. 2. (color online) Reflection characteristics of MS unit M1 for different feeding positions. (a) Phases and (b) magnitudes under x polarization, (c) phases and (d) magnitudes under y polarization.

In order to further explain the wave absorbing property for x-polarized incidence, the current distribution of M1 when $f_{x_1} = 2.8$ mm is presented in Fig. 3 (at reflection frequency 6.0 GHz). Apparently, the current direction on the upper surface of the substrate is different from that on its bottom surface, which implies that there is an interaction between them. Under x polarization, the induced surface current changes its path slightly when flowing through the feeding structure both on the top surface and on the bottom surface. What is more, the current flowing into feeding structure is stronger than that flowing out, which is shown in Fig. 3(a) and also in Fig. 3(b). Therefore, compared with the case under y polarization, the scenario under x polarization shows strong absorption of induced current around the feeding structure.

After being optimized, four MS antenna unit dimensions are confirmed. The specific parameters are exhibited in Table 1, and the relative reflection and radiation performance are shown in Fig. 4. They can be considered as strong absorption of x-polarized incident waves, and total reflection of y-polarized incidence, respectively, as shown in Fig. 4(a). And for x polarization, the four absorption ranges of MS units cover wide bandwidth, which leads to the broadband RCS reduction. Based on the phase cancellation principle, four phase states of MS at 5.52 GHz are well distributed to achieve a desired 2-bit phase resolution under y polarization in Fig. 4(b).

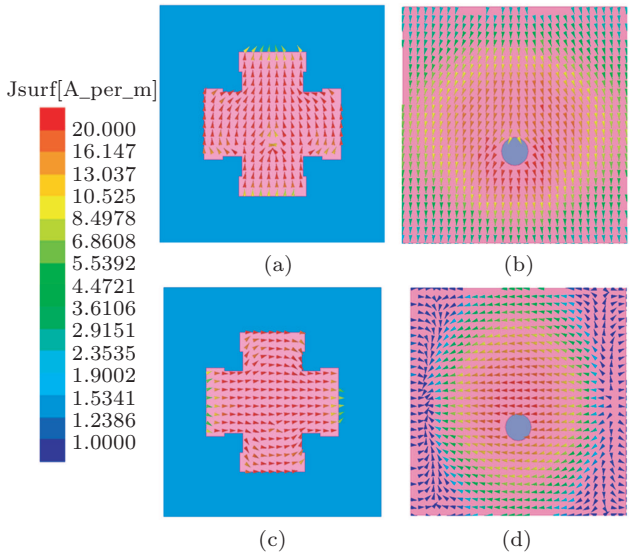


Fig. 3. (color online) Current distributions of M1 at 6.0 GHz on (a) top and (b) bottom surface under x polarization, (c) top and (d) bottom surface under y polarization.

Table 1. Optimized dimensions for MS antenna array.

Parameters	Value /mm	Parameters	Value /mm	Parameters	Value /mm	Parameters	Value /mm
a_1	11.0	a_2	12.5	a_3	9.0	a_4	9.0
b_1	7.5	b_2	8.4	b_3	7.0	b_4	7.0
c_1	6.8	c_2	5.2	c_3	5.0	c_4	5.0
d_1	2.1	d_2	2.0	d_3	2.2	d_4	2.2
f_{x_1}	2.8	f_{x_2}	2.0	f_{x_3}	2.3	f_{x_4}	2.3

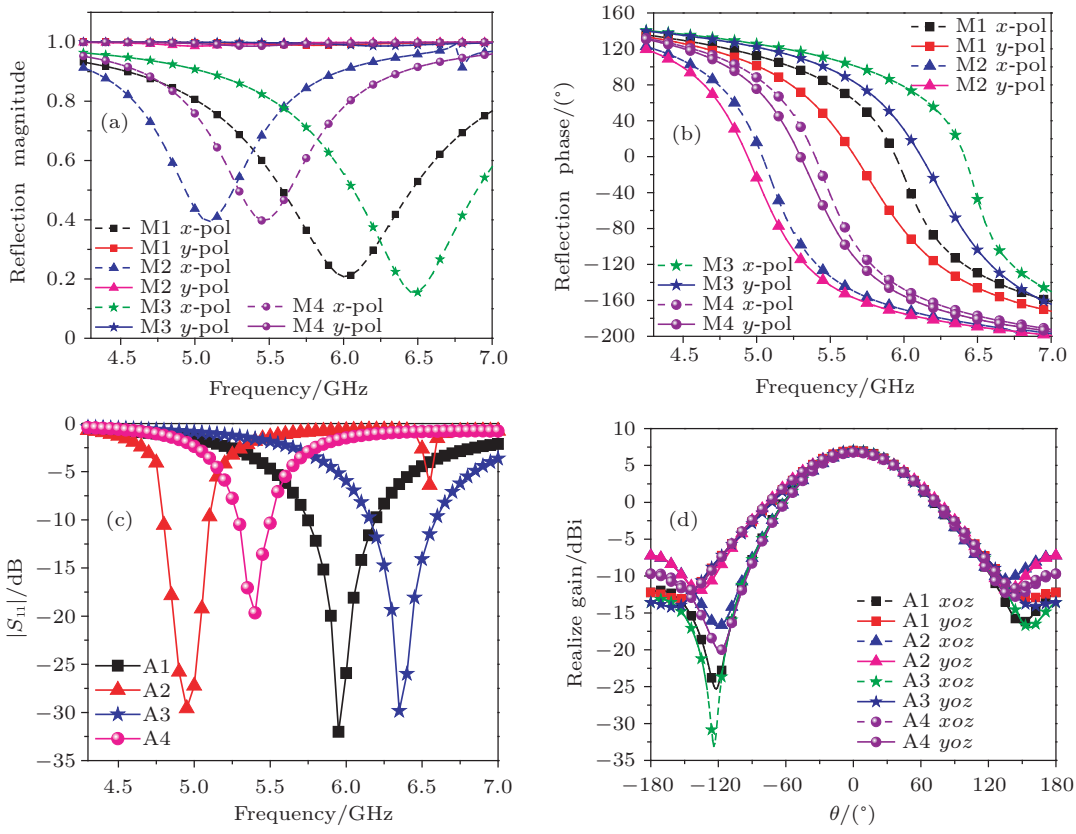


Fig. 4. (color online) Reflection and radiation characteristics of MS antenna unit. (a) Reflection magnitudes, (b) reflection phases, (c) reflection coefficients S_{11}, (d) two-dimensional(2D) radiation patterns.

The fluctuation in phase resolution is less than 15° within a wide bandwidth from 5.30 GHz to 5.75 GHz. For *x*-polarized incidence, the wide frequency range of 180°±30° effective phase difference is also obtained. The reflection coefficients of four antenna units simulated by using radiation boundary are shown in Fig. 4(c). For the four antenna units working at different frequency bands, the multi-band radiation characteristics come true. So the broadening of working bandwidth is realized now. And the radiation patterns of A1–A4, respectively, at 5.95 GHz, 4.95 GHz, 6.35 GHz, and 5.40 GHz, are depicted in Fig. 4(d) From Fig. 4(d) we can see that the peak radiations all happen in the broadside direction under both *x* and *y* polarization. In summary, the simulated results indicate that the proposed MS antenna can integrate radiation and scattering performance simultaneously. As a result, the multi-band properties and good scattering performance can be achieved at the same time.

3. Simulation and analysis of MS antenna array

Based on the passive cancellation technology, four MS antenna units are designed into a chessboard configuration to attenuate the scattering energy as shown in Fig. 5.

The magnitudes of *S* parameter of the antenna array are presented in Fig. 6(a). In the figure, it is clearly revealed

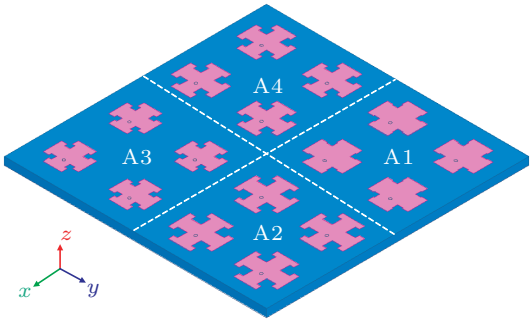


Fig. 5. (color online) Schematic geometry of MS antenna array.

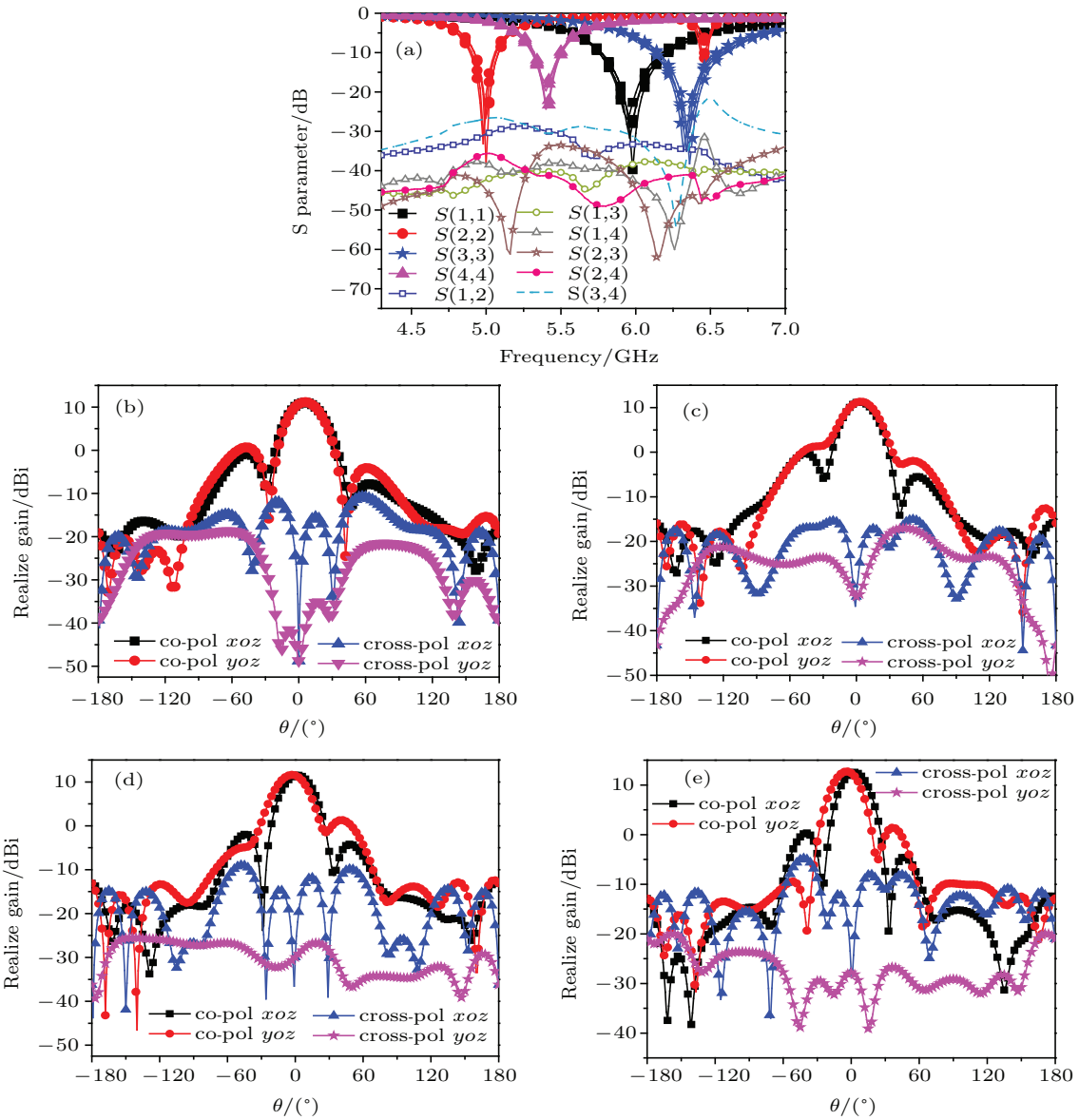


Fig. 6. (color online) Radiation properties of MS antenna array. (a) Reflection and transmission coefficients. 2D radiation patterns at (b) 5.0 GHz, (c) 5.4 GHz, (d) 6.0 GHz, and (e) 6.4 GHz.

that better impedance matching of antennas is obtained after they have been arranged. And for each antenna, the four reflection coefficients have little difference between each other on account of interaction effect among antennas. Therefore, the multi-band property is obtained. The resonant frequencies of array are 5.0 GHz, 5.4 GHz, 6.0 GHz, and 6.3 GHz, respectively, which basically match the results before formation. Moreover, the transmission coefficients in Fig. 6(a) reflect the simulated mutual coupling between different structure units under open boundary condition. The isolation between antenna elements is less than −20 dB in the entire impedance band. In general, the proposed antenna array is able to produce multi-band radiation characteristic and low mutual coupling over a wide frequency range. The corresponding 2D radiation patterns above resonant frequencies are depicted in Figs. 6(b)–6(e). As shown in the figure, the desirable broadside radiation patterns can be observed and the co-polarized fields are 20 dB stronger than the cross-polarized counterparts in the boresight direction. In addition, the side lobe levels are lower bigger-than-10 dB than main lobe levels. In order to visualize the radiation performance at the resonant frequency more intuitively, three-dimensional (3D) radiation patterns are shown in Fig. 7, from which, the MS antenna array exhibits directional radiation patterns with low side lobe levels for all investigated frequencies, so it is evident that good radiation performance is achieved.

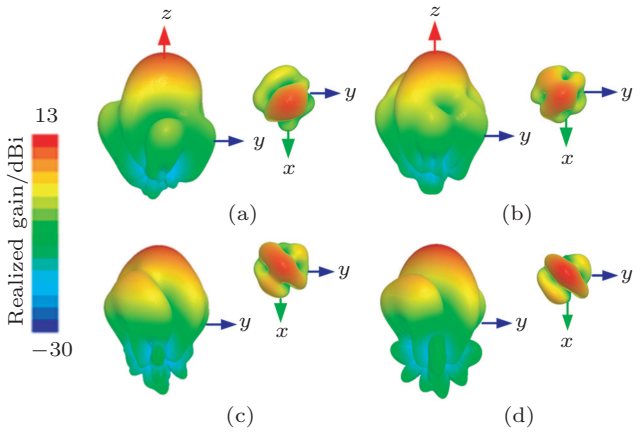


Fig. 7. (color online) 3D radiation patterns of MS antenna array at (a) 5 GHz, (b) 5.4 GHz, (c) 6.0 GHz, and (d) 6.3 GHz.

Figure 8 shows the scattering patterns and mirror RCS reduction curves (they are compared under the condition of the same sized metal ground) at *x* polarization and *y* polarization. It can be observed that a remarkable RCS reduction for normal incident wave covering the operation band is achieved. An evident bistatic specular RCS reduction occurs in a frequency range from 4.3 GHz to 7 GHz when the incident angles (theta) are 0°, 15°, 30°, and 45°. Moreover, 6dB RCS reduction is obtained at frequencies ranging from 5.3 GHz to 6.1 GHz under both *x*- and *y*-polarized incidence. In addition, 3D scattering patterns are given in Fig. 9 to demonstrate that the reflection is diffused in more directions intuitively. Therefore, wideband and wide-angle RCS reduction of MS antenna array is realized.

The comparison between the proposed MS antenna with the existing ones is shown in Table 2. The multi-band characteristic of proposed MS antenna array leads to wideband radiation performance compared with that of previous MS antenna array. And the integrated feature reduces the difficulty in processing. Even though the RCS reduction bandwidth is not particularly wide, it can cover the in-band working range.

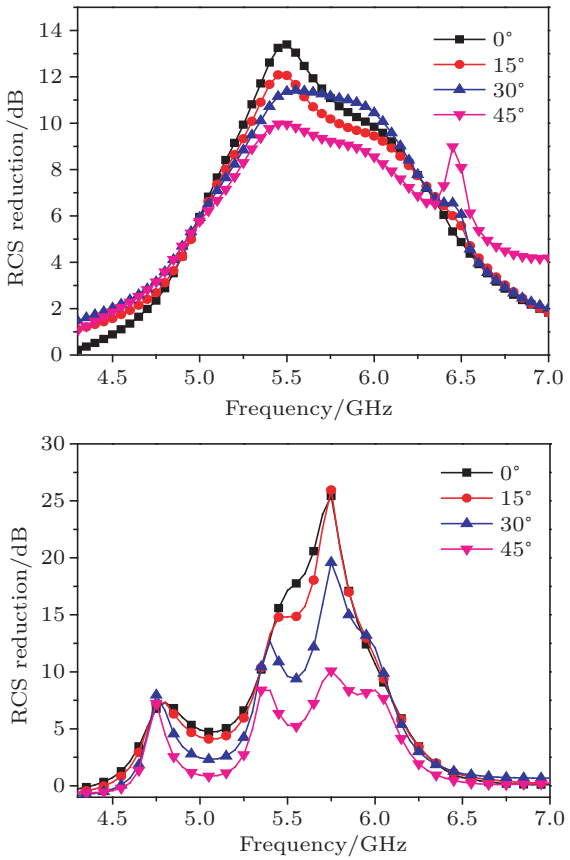


Fig. 8. (color online) RCS reduction of MS antenna array for (a) *x*- and (b) *y*-polarized incidence.

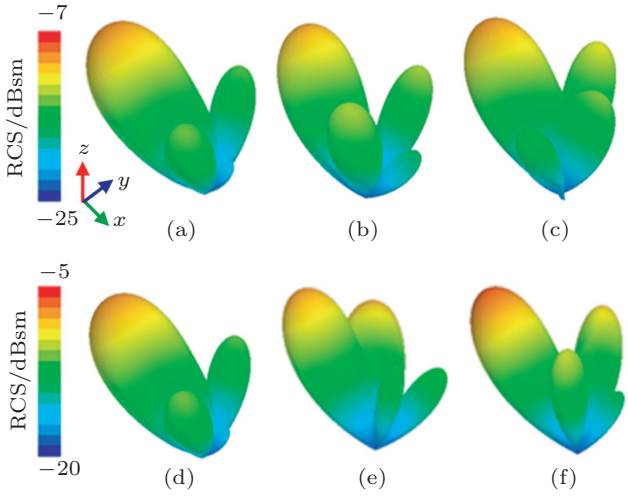


Fig. 9. (color online) Scattering patterns of *x*-polarized incident wave at (a) 5.2 GHz, (b) 5.5 GHz, (c) 6.0 GHz, and of *y*-polarized incident wave (d) 5.0 GHz, (e) 5.5 GHz, and (f) 6.0 GHz.

Table 2. Comparison between different MS antennas.

Absorber	Frequency band number	Fractional bandwidth	Fabrication complexity	Fractional RCS reduction bandwidth
Ref. [12]	single band	8.8%	Complex processing	37.9%
Ref. [15]	dual band	14.1%	Easy processing	46.2%
Ref. [16]	single band	9.3%	Complex processing	88.9%
This paper	multi-band	22.3%	Easy processing	47.8%

4. Fabrication and measurement

To further verify the radiation and scattering performance, a prototype of the MS antenna array is fabricated and measured as shown in Fig. 10.

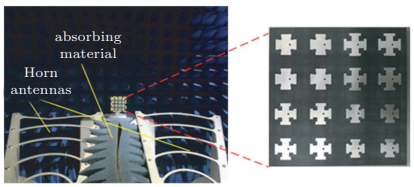


Fig. 10. (color online) Prototype and measurement setup.

The reflection coefficient is measured by a vector network analyzer (VNA), named Agilent N5230C, whereas the gain and the radiation pattern are obtained in the anechoic chamber with two of the eight power dividers RS8W2080-S and one of the two power dividers RS2W2080-S for feeding. The scattering performance is also measured in the anechoic chamber by using the two identical 1 GHz–18 GHz horn antennas connected to the VNA N5230C as receiver and transmitter depicted as shown in Fig. 10.

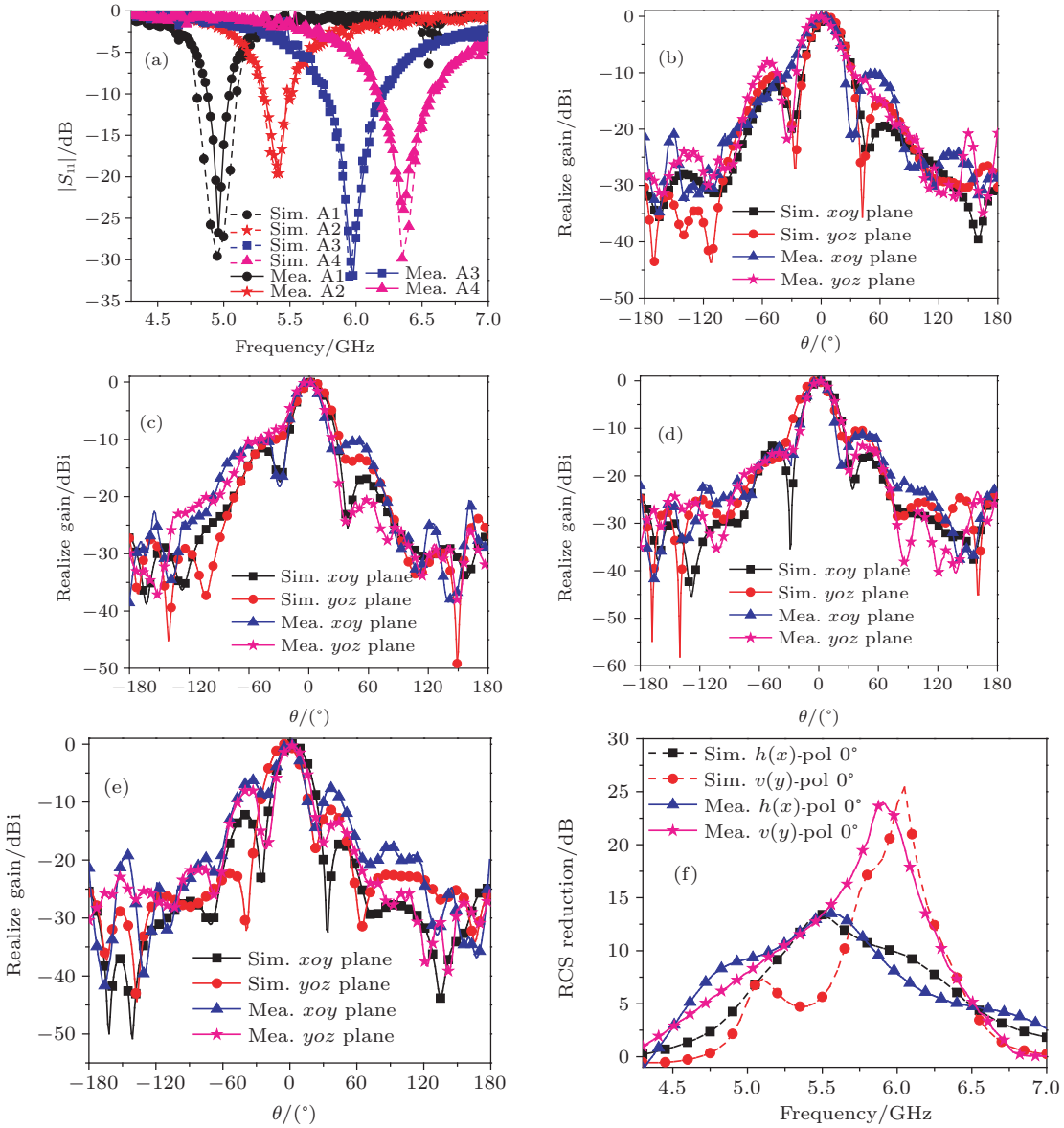


Fig. 11. (color online) Simulated and measured radiation properties and RCS reduction of MS antenna array. (a) Reflection coefficients S_{11}. 2D radiation patterns at (b) 5.0 GHz, (c) 5.4 GHz, (d) 6.0 GHz, and (e) 6.3 GHz. (f) RCS reduction with 0° for x- and y-polarized incidences.

Figure 11 shows the simulated and measured results of radiation and scattering performance. The reflection coefficients are shown in Fig. 11(a), presenting good impedance matching of MS antenna array. And the resonant frequencies approach to 5.0 GHz, 5.4 GHz, 6.0 GHz, and 6.3 GHz, respectively. In contrast to the simulated results, the measured 10dB-bandwidth of A1 turns narrowed slightly. The corresponding 2D radiation patterns at above resonant frequencies are depicted in Figs. 11(b)–11(e). Broadside radiation patterns are observed as expected. The measured side lobe levels are almost 10 dB lower than main lobe levels. Figure 11(f) shows the measured results of RCS reduction curves. On account of the limitation of the testing condition, the measured bistatic RCS cannot be obtained at present. From the results, wideband RCS reduction at 0° is obtained for both x and y polarization, which agrees well with the simulated results. Considering the fabrication and measurement tolerance, the measured results show good agreement with the simulated ones.

5. Conclusions

In this work, a multi-band MS antenna array with low RCS performance is proposed and designed. The 4×4 antenna array is composed of four kinds of antennas working at different frequency bands, which aims at realizing the multi-band property, in order to broaden the bandwidth effectively. Then, each antenna can be seen as a unit of MS. And the inherent characteristics of the MS are maintained well in spite of adding the feeding structure. Based on the phase cancellation principle, the MS is arranged into a chessboard configuration in order to realize wideband RCS reduction of antenna array. Simulation and measurement results verify the feasibility of the proposed MS antenna array. The advantage of this design method is that the MS and antennas are combined together and the radiation and scattering performance are considered simultaneously, which deserves academic concern and study. Additionally, the flexibility of MS units replaced by other geometric structures offers more potential applications in multiple usage.

References

[1] Pereda A T, Caminita F, Martini E, Ederra I, Iriarte J C, Gonzalo R and Maci S 2016 *IEEE Trans. Anten. Propag.* **64** 2944

[2] Minatti G, Faenzi M, Sabbadini M and Maci S 2017 *IEEE Trans. Anten. Propag.* **65** 2836

[3] Lin F H and Chen Z N 2017 *IEEE Trans. Anten. Propag.* **65** 1706

[4] Semenikhin A I, Semenikhina D V, Yukhanov Y V and Blagovisnyy P V 2017 *ICEAA* 360

[5] Zheng Y J, Gao J, Cao X Y, Yuan Z D and Yang H H 2015 *IEEE Anten. Wireless Propag. Lett.* **14** 1582

[6] Zheng Y J, Gao J, Xu L M, Cao X Y and Liu T 2017 *IEEE Anten. Wireless Propag. Lett.* **16** 1651

[7] Baskey H B and Akhtar M J 2017 *IEEE Trans. Microwave Theory Tech.* **65** 2019

[8] Su P, Zhao Y, Jia S, Shi W and Wang H 2016 *Sci. Rep.* **6** 20387

[9] Yang W, Wang H, Che W and Wang J 2013 *IEEE Anten. Wireless Propag. Lett.* **12** 769

[10] Cui T J, Qi M Q, Wan X, Zhao J and Cheng Q 2014 *Light Sci. Appl.* **3** 1

[11] Su J X, Kong C Y, Li Z R, Yin H C and Yang Y Q 2017 *Electron. Lett.* **53** 1088

[12] Long M, Jiang W and Gong S X 2017 *IEEE Anten. Wireless Propag. Lett.* **16** 2534

[13] Li K, Liu Y, Jia Y T and Guo Y J 2017 *IEEE Trans. Anten. Propag.* **65** 4288

[14] Ta S X and Park I 2017 *IEEE Anten. Wireless Propag. Lett.* **16** 1932

[15] Zheng Y J, Cao X Y, Gao J, Yang H H, Zhou Y L and Liu T 2017 *Opt. Express* **25** 30001

[16] Mu J, Wang H, Wang H Q and Huang Y 2017 *IEEE Anten. Wireless Propag. Lett.* **16** 1903